Effect of surface integrity generated by machining on isothermal low cycle fatigue performance of Inconel 718

A. Madariaga[a], A. Garay[a], J.A. Esnaola[a], P.J. Arrazola[a], A. Linaza[b]

[a] Mechanical and Industrial Production Department, Faculty of Engineering, Mondragon Unibertsitatea, Loramendi 4, Mondragon 20500 Gipuzkoa, Spain

[b] Materials and Processes Technology department, ITP Aero, Parque Tecnológico, Edificio 300, 48170 Zamudio, Spain

[*]Corresponding author. Tel.: +34 943 71 22 74; Fax: +34 943 711 912

e-mail address: amadariaga@mondragon.edu (A. Madariaga)

Abstract

Critical aero-engine components such as turbine discs must withstand severe cyclic stresses, which can eventually lead to low cycle fatigue (LCF) failures. These components are made of difficult-to-cut alloys and machining conditions that are employed in the last stage of the manufacturing chain must be correctly defined to avoid the generation of an adverse surface condition (tensile residual stresses, excessive surface roughness or microstructural defects) that will accelerate fatigue failure. The analysis presented in this paper is aimed at understanding the isothermal LCF behaviour of turned Inconel 718 workpieces and finding quantitative correlations with the surface integrity. For this purpose, two Inconel 718 forged discs were face turned at cutting conditions employed in the aero-engine manufacturing industry using two different tools (1.2 mm and 4 mm nose radius respectively). The surface integrity produced by the face turning process was characterised in both discs: surface topography, residual stresses and surface layer anomalies. Specimens extracted from both discs were tested in load control at 450 ºC to obtain LCF fatigue behaviour. Importantly, interrupted isothermal LCF fatigue tests were conducted and residual stresses were measured by the X-ray diffraction technique at the surface of the tested specimens to study the role of residual stresses in the LCF fatigue behaviour. For the tested conditions, the specimens machined with 4 mm nose radius showed 1.3-1.4 times longer fatigue lives than the specimens turned with 1.2 mm nose radius. These results are in agreement with the better surface integrity generated with the 4 mm nose radius, mainly because it induced lower tensile residual stresses. A novel local approach was implemented to understand the influence of surface integrity (surface roughness, surface residual stresses and altered stress-strain properties of the surface layer) on the isothermal LCF fatigue behaviour of both machined discs. Interestingly, a satisfactory correlation was found between the maximum applied stress in the surface layer and the isothermal LCF fatigue life employing the local approach.

Keyword: fatigue, surface integrity, X-ray analysis, nickel alloys, machining

1. Introduction

Aero-engine components are classified into ‘critical’ or ‘non-critical’ depending on the consequences that a malfunction might have on the integrity of the aircraft [1]. Particularly, turbine discs are one of the most critical components and they are usually made of nickel based alloys if they have to withstand high temperatures. These components possess enormous kinetic energy, especially during the take-off sequence. Such operations induce severe cyclic stress which can eventually lead to low cycle fatigue failures [1]. Consequently, a failure of a turbine disc will result in the uncontained release of large pieces of metal with extremely high energy and damage the aircraft. The 1997 report of the AIA Rotor Integrity Committee stated that about 25% of rotor failure events are caused by manufacturing induced anomalies [2]. Thus, meticulous manufacturing of such parts is critical to ensure airworthiness and passenger safety.

The last stage of the manufacturing chain is usually where the machining operations of critical aero-engine components such as turbine discs are carried out. These parts are made of difficult-to-cut alloys, due to their characteristics during the cutting process [3]: low thermal conductivity, prone to work-hardening, retention of high strength levels at high temperatures and presence of abrasive carbides in their microstructure. If machining process parameters are not selected appropriately, the surface integrity (SI) of the machined components can be affected (this includes microstructural damage, excessive surface roughness and surface tensile residual stresses). Thus, stringent controls are placed on the manufacturing of critical components to ensure correct performance and safety along the service life [2].

In this context, a number of research studies have analysed the SI after machining aero-engine alloys over the last decade as summarised in recent literature reviews [4, 5]. Although these efforts have enabled understanding the influence of machining conditions on the SI of nickel based alloys, the correlation between SI and in-service fatigue behaviour is not widely understood.

It is generally accepted that surface anomalies generated during machining are detrimental to fatigue life of nickel based alloys. Connolley and co-workers [6] studied the effect of broaching on fatigue behaviour of Inconel 718. They observed that the broaching process that led to more severe deformation showed the worst fatigue performance although surface roughness was lower. Bhowal et al. [7] studied the impact of several surface conditions on LCF behaviour of specimens extracted from direct aged forged Inconel 718 discs. They reported that conventional machining processes (turning and boring) cracked or damaged surface carbides leading to shorter crack initiation periods and consequently reducing their LFC life. Welling [8] also found that carbide break outs on broached surfaces reduced the fatigue life of Inconel 718 specimens. Herbert et al. [9] analysed the influence of surface defects generated when hole making the nickel based alloy RR1000 on its fatigue life. They found that specimens with white layers and material drag exhibited significantly lower fatigue life compared to damage free specimens. Some other authors have reported that the recast layer and craters generated by electro discharge machining affect negatively to the fatigue performance of nickel based alloys [8, 10, 11].

Surface roughness is another major parameter affecting the fatigue performance of machined components. Huang and Ren [12] compared the HCF and LCF fatigue performance of specimens of the nickel based alloy GH33A produced by rough turning, fine turning and grinding. They found that under the condition of LCF surface roughness was the main factor as residual stresses relaxed due to plastic strains and thermal exposure. Connolley et al. [6] demonstrated that polishing the notch improved the fatigue performance of broached specimens of Inconel 718, which evidenced that fatigue lifetimes were also affected by surface roughness. Nevertheless, other researchers [13, 14] have found that HCF and LCF fatigue of nickel based alloys Inconel 718 and Alloy 720 were insensitive to surface roughness when R_a is lower than 5 μm.

In one pioneering work Koster et al. [15] compared the HCF fatigue performance of solution treated and aged Inconel 718 after machining with different processes: gentle grinding, conventional

grinding, roughing EDM, finishing EDM, gentle ECM, abusive ECM and ELP. They found a good agreement, not conclusive, between peak surface or subsurface and fatigue strength. Later, Galatolo and co-workers [16] analysed the effect of SI on fatigue behaviour of Inconel 718 specimens turned at three different conditions. For the tested conditions, the effect of residual stresses dominated over those of microstructure defects and surface roughness. More recently, Hua and Liu [17] also studied the effect of residual stresses generated by turning on fatigue performance of Inconel 718. They found that the maximum principal residual stress can be considered as prime indicator for evaluation of the residual stress impact on the fatigue performance of machined components. Nevertheless, none of these works analysed the relaxation of residual stresses under thermomechanical loads. In fact, to quantify the real effect of residual stresses on the fatigue life, it is necessary to understand the changes of machining-induced residual stresses under mechanical and thermal loading, which depend on the local mechanical properties (stress-strain curve) of the surface layer [18].

As explained in the preceding paragraphs, several works have been published analysing the effect of various machining processes on the fatigue life of nickel based alloys. Although these studies have allowed understanding the influence of machining on HCF and LCF fatigue behaviour of these alloys, there is limited information correlating machining parameters with surface integrity and fatigue performance. As discussed in the literature review, there is not one major parameter of the surface integrity influencing on the fatigue life of machined components; many authors others have identified surface roughness or surface damage to be the most important, whilst some others have found machining induced residual stresses to be the most relevant parameter. Unfortunately, none of the previously reported works have studied the relaxation of residual stresses due to thermal and mechanical loads which is a key parameter to quantify the effect of residual stresses on the fatigue strength. Therefore, further research is required in order to obtain a better understanding and quantitative relationship of machining conditions, surface integrity and fatigue behaviour.

The analysis presented in this paper is aimed at understanding the isothermal LCF behaviour of turned Inconel 718 workpieces and finding quantitative correlations with the surface integrity. For this purpose, two Inconel 718 forged discs were face turned at cutting conditions employed in the aero-engine manufacturing industry using two different tools. The surface integrity produced by the face turning process was characterised in both discs: surface topography, residual stresses and surface layer anomalies. Specimens extracted from both discs were tested in load control at 450 ºC in order to obtain LCF fatigue behaviour. Importantly, interrupted isothermal LCF fatigue tests were conducted and residual stresses were measured at the surface of the tested specimens aimed at analysing the role of residual stresses in the LCF fatigue behaviour.

2. Material and Experimental Procedure

2.1. Material

Two 7 mm thick Inconel 718 forged discs with an average grain size of ASTM 9 were used in this study. The chemical composition of the forged material can be seen in Table 1. Figure 1 shows the microstructure of the material which consists of an austenitic face centred cubic matrix with gamma double prime γ'' strengthening precipitates.

Table 1. Chemical composition (%wt) of the Inconel 718 forging disc.

Ag	Al	B	Bi	C	Co	Cr	Cu	Fe	Mg
<=0.001	0.4-0.8	<=0.006	<=0.00003	0.02-0.07	<=1.00	17-21	<=0.1	Balance	<=0.003
Mn	Mo	Ni	Nb+Ta	P	Pb	S	Si	Ti	
<=0.35	2.8-3.3	50-55	5.0-5.5	<=0.015	<=0.0005	<=0.008	<=0.35	0.65-1.15	

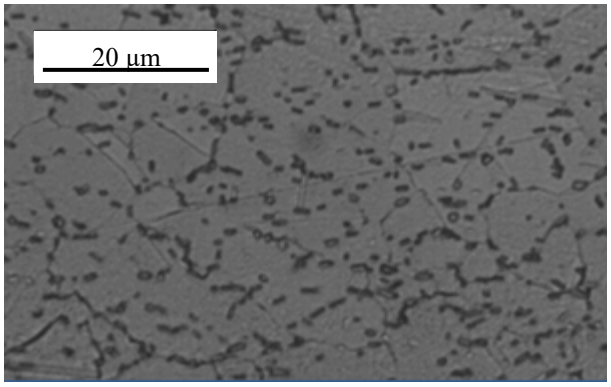

Figure 1. Microstructure of the Inconel 718 forged material.

2.2.Machining tests and specimen preparation

First of all the 7 mm thick Inconel 718 forged discs were cut by wire electro discharge machining process to obtain a ring shape part. Then, both ring shape parts were face turned in a Danobat vertical lathe. Discs were machined employing two different coated carbide tools: 4 mm nose radius (tool A) and 1.2 mm nose radius (tool B).

Machining of both discs was carried out using identical cutting strategy and conditions to the ones used in the aero-engine manufacturing industry. The upper and lower surface of each disc was face turned with a fresh tool through three passes, reducing the intermediate section to 4 mm thickness, as represented schematically in Figure 2.

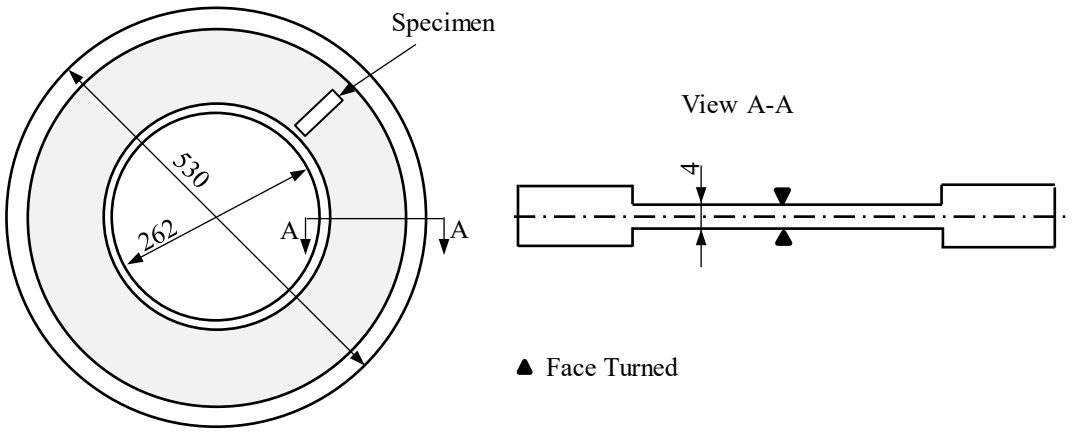

Figure 2. Scheme of the machined ring and specimen location.

Then, specimens for LCF tests were extracted by electro discharge machining from the intermediate area (grey area) of both discs. The longitudinal axis of the specimens was aligned with radial direction of the ring, as can be seen in Figure 2. The specimens were finally prepared: edges were rounded and sides were ground to remove the recast layer produced by the EDM process. Figure 3 shows the geometry of the specimens.

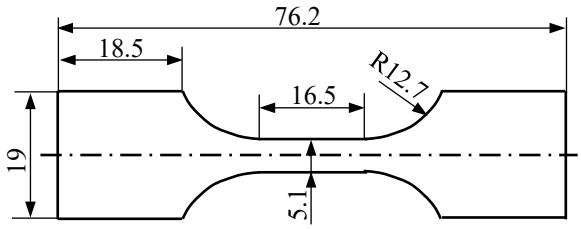

Figure 3. Geometry of specimens for isothermal LCF fatigue tests. Dimensions in mm.

2.3.Surface roughness measurements

A portable Mitutoyo SJ-210 roughness meter was used to characterise the surface topography of both machined discs. The following parameters were measured on the final surface of the machined discs: average surface roughness R_a, maximum peak to valley height R_t, average peak to valley height R_z, root mean square roughness R_q, the value of the highest single peak above the centre line R_p and the mean spacing of the profile R_{sm}. Measurements were repeated five times on the surface of each disc at different locations and average value was calculated for the subsequent surface integrity analysis.

2.4.Residual stress measurements

Residual stresses were measured at the surface of the specimens using the X-ray diffraction method before and after interrupted isothermal LCF fatigue tests. The X-ray diffraction technique allowed repeating measurements of residual stresses at the same point of each specimen before and after interrupted isothermal LCF fatigue tests. Surface residual stresses were measured in the centre of the specimens shown in Figure 3 in the longitudinal direction. A Bruker D8 advance diffractometer was used for this purpose (see Figure 4). The radiation employed was CrKα1 (λ=2.291 Å), with

voltage of 40 kV and current of 4 mA. The (2 2 0) diffraction plane of the austenitic matrix was chosen for the measurements. A round collimator (2 mm diameter) on the incident beam was used. Measurements carried out in Ω mode with 9 inclinations and experimental data were analysed by means of Diffrac software. Diffraction peaks were fitted with a Pearson VII function that is necessary for eliminating errors from varying blending and defocusing of the Kα doublet diffraction peak [19]. The diffraction elastic constants used in the measurements were the following: $-S_1=1.401\cdot10^{-6}$ [MPa^{-1}], ½ $S_2=6.232\ 10^{-6}$ [MPa^{-1}].

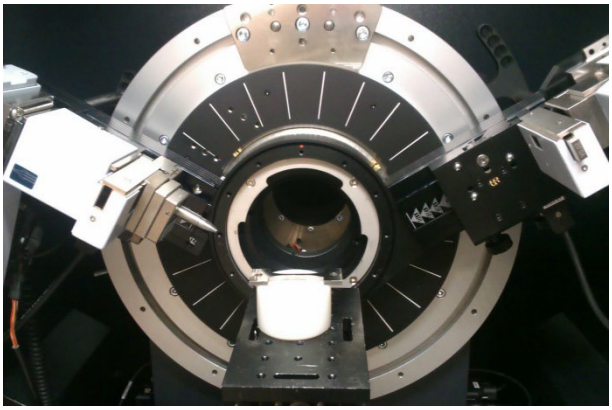

Figure 4. Set-up of a specimen in the Bruker D8 advance diffractometer.

2.5.Microscopy observations: surface layer anomalies

Specimens for microstructural observations were cut by wire electro discharge machining from the face turned discs or employing the metallographic saw. These specimens were hot mounted in a phenolic resin with carbon filler, ground employing Silicon Carbide papers and polished to obtain the desired surface quality. Then, specimens were chemically etched using a Grandy solution. The microstructure of the specimens was observed in a Leica DM IRM optical microscope.

2.6.Isothermal low cycle fatigue tests

Isothermal low cycle fatigue tests were conducted according to ASTM E466 07 in load control at 450 ºC, employing a closed loop servo controlled hydraulic MTS machine of 100 kN capacity and an induction heating system. Eight specimens, geometry shown in Figure 3, were extracted from each

disc. They were tested at three maximum nomimal stress levels (S_{max1}, S_{max2}, S_{max3}) near the yield stress of the material using a trapezoidal wave (1-1-1-1) and stress ratio R=0. Tests were run upon specimen rupture.

Once specimen failure had occurred, a full fractographic analysis was carried out. Firstly, the fractured section of all tested specimens was observed in a macroscope. After that, representative specimens from both batches were selected to analyse in greater detail within a SEM. For that purpose, the selected specimens were first cleaned in acetone using an ultrasonic bath for half an hour.

2.7.Interrupted isothermal low cycle fatigue tests

In order to study the influence of machining induced residual stresses on the isothermal LCF fatigue behaviour additional interrupted fatigue tests were performed. Firstly, surface residual stresses were measured by the X-ray diffraction method in the centre of the upper and lower surface of the specimens of both discs. Then, specimens from both discs were tested at S_{max1} and S_{max3} maximum nomimal stress levels during 1 cycle and cooled in air. After that, surface residual stresses were measured in the centre of the specimens. Finally, the specimens were tested again at the same S_{max1} and S_{max3} maximum nominal stress levels for 1000 cycles and cooled in air before performing final surface residual stress measurements.

3. Results

3.1.Surface roughness

Table 2 shows the results obtained in the surface roughness measurements. The two main machining parameters influencing on the surface roughness are the feed rate and the tool nose radius. In this study, the feed rate was identical when face turning both discs, but the tool geometry was changed. As can be seen in Table 2, R_a, R_t, R_z, R_q and R_p were four times higher when machining with the smallest nose radius. Therefore, the surface produced with the 1.2 mm nose radius tool was significantly rougher than the surface machined with the 4 mm nose radius tools.

Table 2. Surface topography results for both discs at different machining steps.

Nose radius [mm]	R_a [µm]	R_t [µm]	R_z [µm]	R_q [µm]	R_p [µm]	R_{sm} [µm]
1.2	1.2	5.6	5.1	1.4	2.7	155.1
4	0.3	2.0	1.8	0.4	0.8	202.7

3.2. Initial surface residual stresses

Initial surface residual stresses were measured by the X-ray diffraction method in the longitudinal direction in the centre of the specimens obtained from both discs. Figure 5 shows the results of surface residual stress values, which have been normalized with respect to the highest initial surface residual stress value. Both tools produced tensile residual stresses in the surface layer, which indicates that the effect of thermal loads generated during the machining was higher than the effect of mechanical loads of the cutting process. On average, 30 to 40 % higher surface residual stresses were measured in the longitudinal direction of the specimens machined with the 1.2 mm nose radius tools than at the surface machined with the 4 mm nose radius tool.

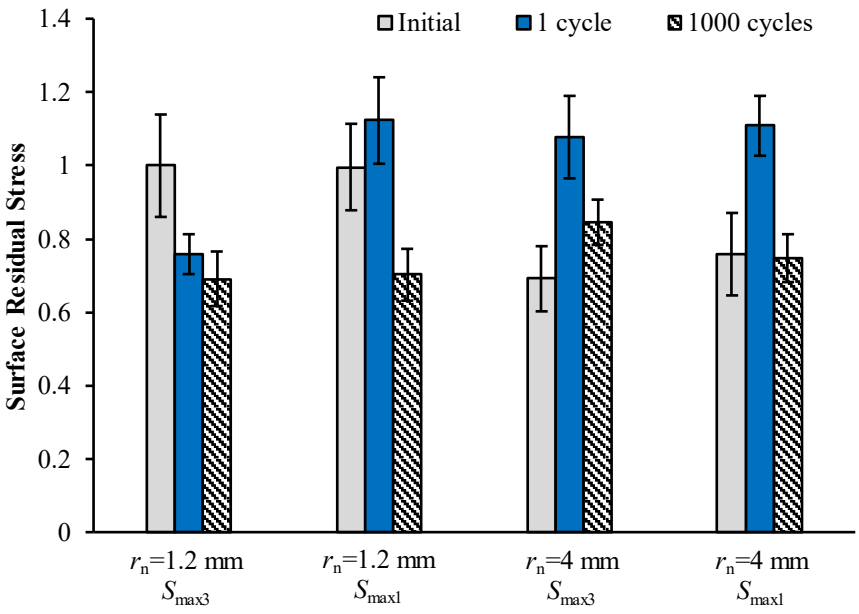

Figure 5. Initial surface residual stress, after the first loading cycle and after 1000 loading cycles.

3.3.Surface layer anomalies

Both discs machined with 1.2 mm and 4 mm nose radius tools respectively, presented similar defects. Distorted layer and strain hardening were the main defects found in the surface layer of both discs. These anomalies were observed in localised regions of the machined surfaces. Furthermore, the depth of the altered microstructure was very little, as shown in Figure 6. For instance, the depth of the maximum distorted layer was below 6 µm and the thickness of the strain hardened layer did not exceed 10 µm at the final surface (intermediate region of the discs). These values satisfy the requirements defined by the aero-engine manufacturers (maximum allowable depth for distorted layers and strain hardened layers).

a)

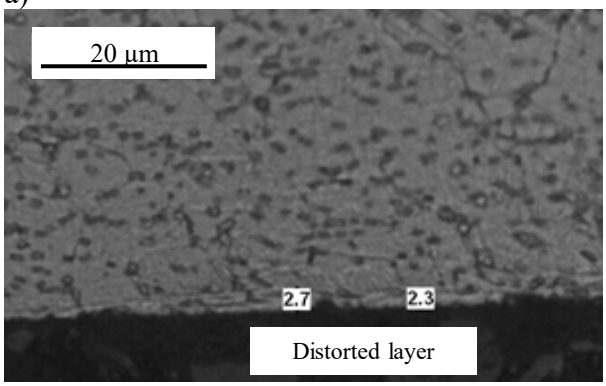

b)

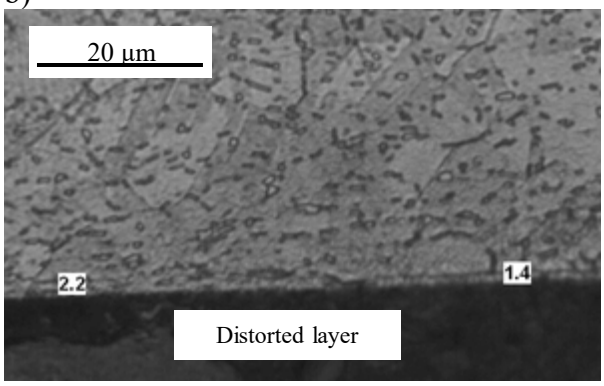

c)

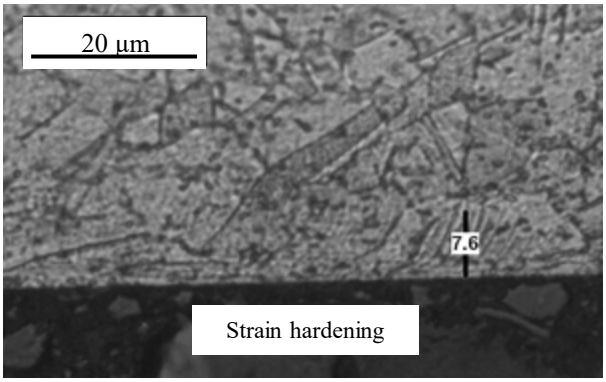

Figure 6. Examples of main surface anomalies found in the machining affected layer; a) distorted layer after machining with the 1.2 mm nose radius tool, b) distorted layer and c) strain hardening when machining with the 4 mm nose radius tool.

3.4.Isothermal low cycle fatigue

The results of isothermal low cycle fatigue tests for both discs are plotted in Figure 7. It should be clarified that one specimen from the disc machined with 4 mm nose radius exhibited much longer fatigue life (open circle) than the rest of specimens at the same level. In particular, this specimen was employed during the calibration of the test temperature, and therefore, tensile residual stresses were probably thermally relaxed leading to longer fatigue life. As can be seen in the graph, specimens machined with 4 mm nose radius showed longer fatigue lives at any applied stress, except one isolated specimen at S_{max2} applied stress. If we compare the shortest lives at each maximum applied stress level, the fatigue life provided by specimens machined with the 4 mm nose radius was 1.5 times longer at S_{max3}, 1.4 times longer at S_{max2} and 1.3 times longer at S_{max1} than fatigue life of specimens machined with 1.2 mm nose radius.

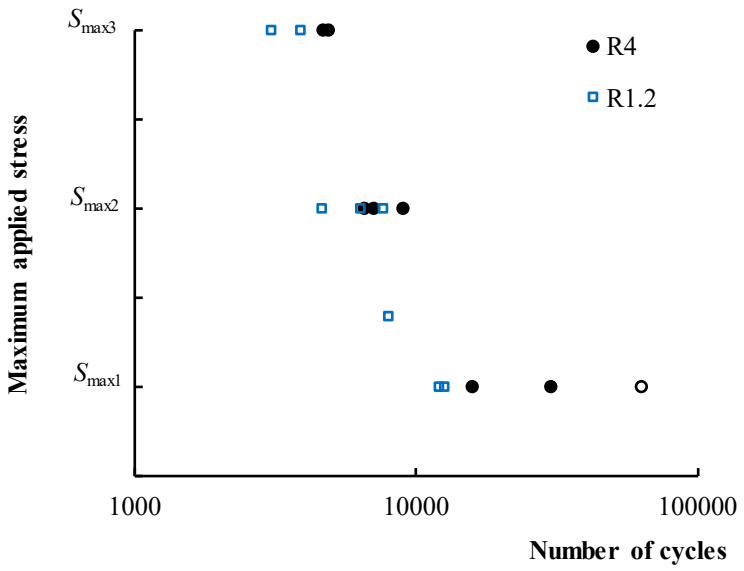

Figure 7. Maximum applied stress vs number of cycles for the low cycle fatigue tests at 450ºC.

Figures 8a and Figure 8b show the fractures of the specimens from the discs machined with 1.2 mm nose radius and 4 mm nose radius tools respectively, observed with the macroscope. As can be seen in the images, a predominant single crack was observed at the lowest applied load in the specimens from the two batches. However, at the highest applied load the fractured surfaces showed multiple crack nucleation sites as it is expected under low cycle fatigue tests when high loads are applied.

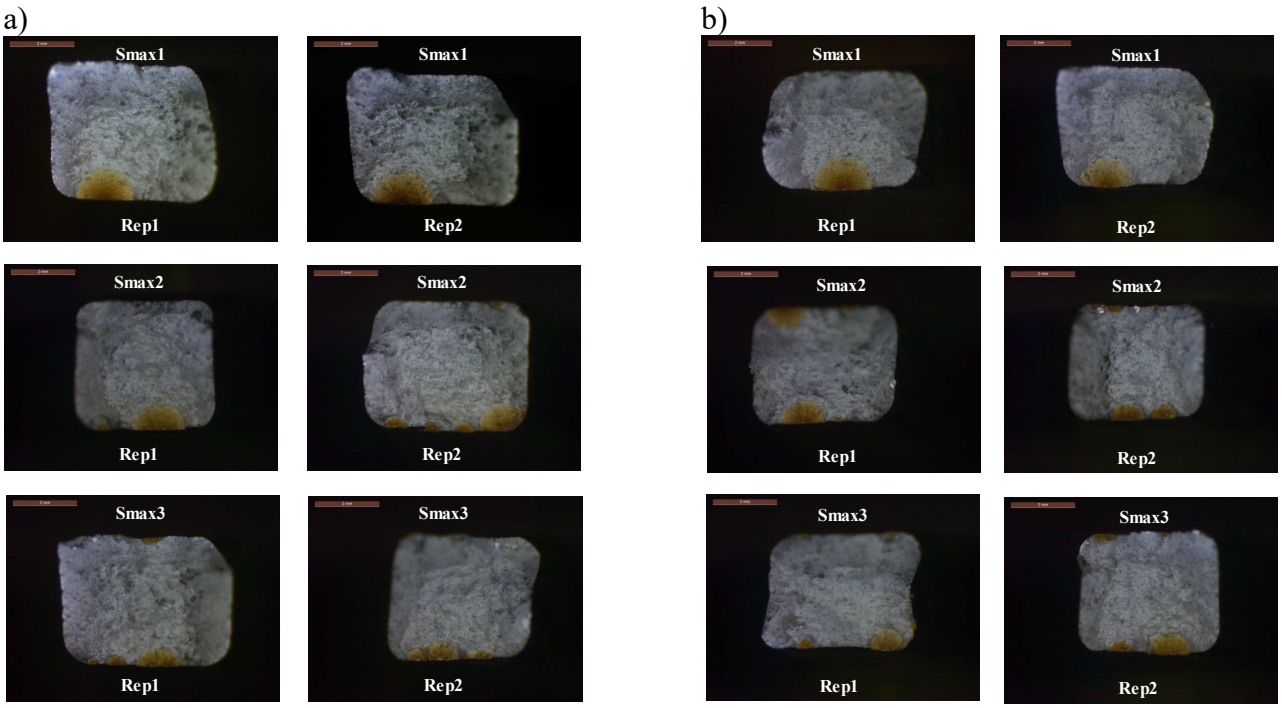

Figure 8. Macroscopic images of the fractures of the specimens machined with a) 1.2 mm nose radius tools and b) 4 mm nose radius tools.

As mentioned in the methodology section, representative specimens from both batches were selected to observe in greater detail within a SEM. They confirmed that cracks were nucleated in the machining affected layer, at the very surface or within a depth of 10 µm. Figure 9 shows SEM micrographs, at different scales, of the fractured surface of one specimen from the disc machined with the 1.2 mm nose radius tool tested at S_{max3} applied load. As can be seen in Figure 8 the primary crack, also the secondary cracks, was initiated at the surface. Although the absence of significant defects close to the surface, the presence of a severe deformed layer (7 µm thick) could have promoted the crack initiation and early propagation period. Figure 10 shows another example of SEM micrographs, at different scales, of the fractured surface of one specimen from the disc machined with the 4 mm nose radius tool tested at S_{max3} applied load. As can be seen, the main features of this fracture are identical: crack initiated at the surface with presence of a severe deformed layer (5 µm thick). Although some authors [7,8] have reported reduction of fatigue live of machined specimens due to carbide break

outs, none of the cracks observed in the present work was nucleated in crack carbides, neither at the surface or in the bulk. Therefore, the fatigue crack initiation was dominated by the surface state.

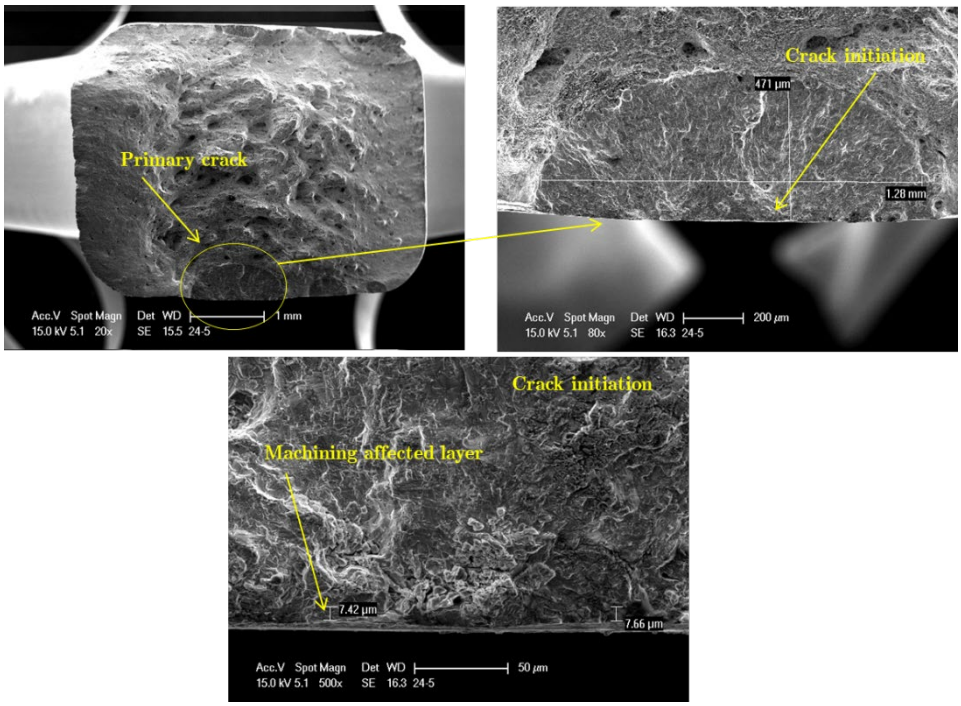

Figure 9. SEM micrographs of the fracture of one specimen from the disc machined with the 1.2 mm nose radius tool tested at S_{max3} applied load.

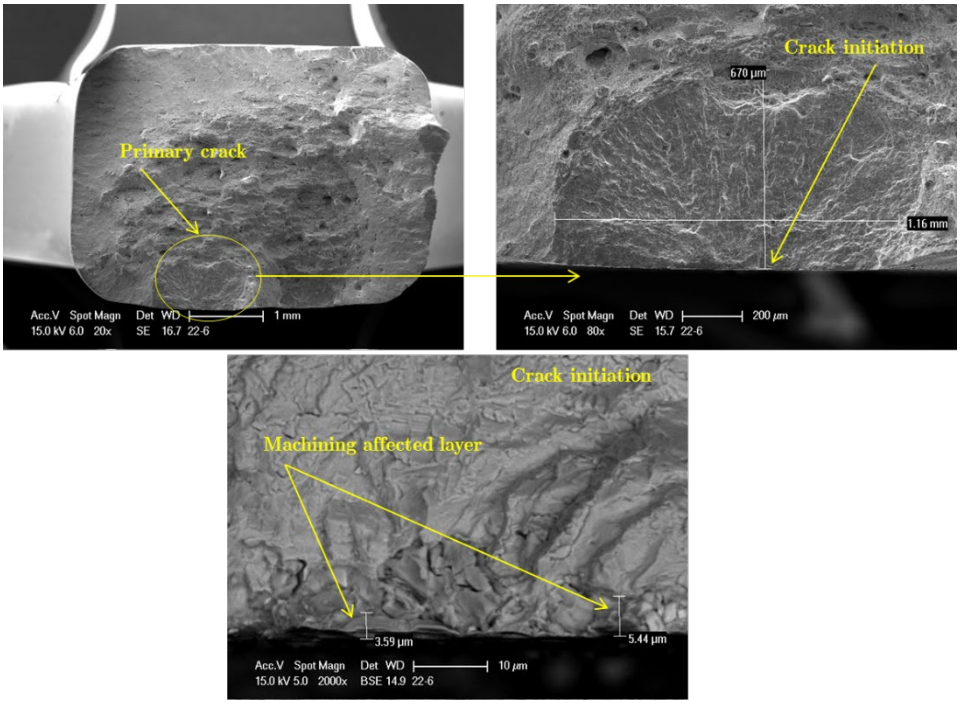

Figure 10. SEM micrographs of the fracture of one specimen from the disc machined with the 1.2 mm nose radius tool tested at S_{max3} applied load.

The shortest lives obtained by the specimens machined with the 1.2 mm nose radius are in agreement with the surface integrity of the specimen (the specimens were extracted from the intermediate area of the discs). The main anomalies found in the surface layer of both discs were strain hardened and distorted layers. These anomalies were observed in localised regions and did not exceed 10 μm in depth, which are far below from the acceptance limit established by aero-engine manufacturers. Therefore, the effect of surface anomalies could be considered as no significant. Nevertheless, surface roughness and tensile residual stresses were higher in the disc machined with the 1.2 mm nose radius tool. Thus, it seems plausible to obtain lower fatigue lives because rougher surfaces and tensile stresses reduce the fatigue strength.

4. DISCUSSION

As described in the preceding section, the primary cracks were nucleated near the surface and were dominated by the surface state. In the following paragraphs the effect of surface roughness and residual stresses on LCF life is discussed in detail, and a Local Fatigue approach that takes into account the surface state (roughness, residual stresses and stress-strain curve of the surface layer) is proposed.

4.1.Effect of surface roughness

As already discussed, the surface roughness R_a, R_t, R_z, R_q and R_p were four times higher when machining with the 1.2 mm nose radius tool. Most of the researches indicate that fatigue life increases when decreasing surface roughness [20]. However, surface roughness standard parameters do not always give an accurate fatigue life reduction prediction [21].

Neuber in 1958 stated that a rough surface should be considered as multiple notches all together [22]. He propounded a semi empirical expression for the stress concentration factor k_t (eq.1), taking into account roughness R_z and profile valley radius ρ. Parameter n defines the stress state (n=1 shear and n=2 tensile) and λ represents the ratio between peak to peak distance and the height of irregularities (in practice, λ = 1 is considered an appropriate value).

$$k_t = 1 + n\sqrt{\lambda \frac{R_z}{\rho}} \quad \text{(eq.1)}$$

Once k_t is determined, fatigue stress concentration factor k_f can be obtained by equations 2, 3 and 4, where σ_u is the rupture stress of the material.

$$k_f = 1 + q\left(k_t - 1\right) \quad \text{(eq.2)}$$

$$q = \frac{1}{(1 + \gamma / \rho)} \quad \text{(eq.3)}$$

$$\gamma = 0.025\left(\frac{2070\text{MPa}}{\sigma_u}\right)^{1.8} \quad \text{(eq.4)}$$

Table 3 shows the fatigue stress concentration factors for the fatigue specimens of both batches calculated based on Neuber's approach (k_{fN}). It should be mentioned that the radius of the valley was not measured. However, in nose turning, as at the present study, the profile valley radius is close to the tool nose radius, at least when tools show little wear. Therefore, the tool nose radius was selected as the profile valley radius. Neuber's approach determined 12% higher fatigue stress concentration factor in the specimens machined with 1.2 mm nose radius which could explain the effect of surface roughness on the LCF fatigue life of the machined specimens.

Table 3. Fatigue stress concentration factors calculated based on Neuber's approach.

Nose radius (mm)	Step	R_a (µm)	R_t (µm)	R_z (µm)	k_{fN}
1.2	Final	1.2	5.6	5.1	1.125
4	Final	0.3	2.0	1.8	1.002

4.2.Effect of residual stresses

As explained in section 3.2., surface residual stresses were 30-40% higher in the specimens machined with the 1.2 mm nose radius tools, which also explain the shorter LCF exhibited by these specimens.

As described in the methodology (section 2.7), interrupted isothermal LCF were conducted to understand the evolution of residual stresses during cyclic loading and evaluate their real influence on the isothermal LCF fatigue behaviour of the machined specimens. Figure 5 shows the initial surface residual stresses and the surface residual stress after applying one cycle and 1000 loading cycles.

The initial surface residual stresses decreased in the specimen machined with the 1.2 mm nose radius tool after applying one loading cycle at S_{max3}, as can be observed in Figure 5. By contrast, initial surface residual stresses increased in the rest of cases after the first loading cycle. Residual stress increase or decrease depending on the difference between the surface yield stress and core yield stress $(\sigma_{y,surf} - \sigma_{y,core})$ [18, 23]. When an external load is applied over the yield stress, surface layer begin to deform plastically in the longitudinal direction before the core region and initial surface residual stresses are relaxed. Therefore, it can be concluded that the surface of the specimens machined with the 1.2 mm nose radius tool experienced higher plastic strain than the core region after applying the first loading cycle at S_{max3}. By contrast, the surface of the three other cases suffered lower plastic strain than the core region.

Surface residual stresses decreased in all cases during the subsequent 1000 loading cycles as can be seen in Figure 5. The decrease in surface residual stresses can be mainly attributed to the material softening that occurred as a consequence of cyclic loading. In addition, surface residual stress relaxed due to the thermally activated processes. Taking into account that nickel-based alloys have good creep properties even up to 75% of the melting temperature [24], the relaxation of residual stresses due to the thermally activated process at 450 ºC was very low (this temperatures below the 40% of the melting temperature of Inconel 718). In fact, recently, we analysed the thermal relaxation

of machining induced residual stresses in Inconel 718 and based on the Zener-Wert-Avrami model fitted in [25] estimated 10% of relaxation at 450 ºC after 50 hours of exposure.

Surface residual stresses were slightly higher (≈10%) in the specimens machined with the 4 mm nose radius tools than in the specimens machined with the 1.2 mm nose radius tool after 1000 loading cycles (see Figure 5). This finding suggests that the isothermal LCF fatigue life of specimens machined with the 4 mm nose radius tool would be lower. However, isothermal LCF fatigue tests showed the opposite trend. These results can be explained based on the first loading cycle. Indeed, specimens machined with the 1.2 mm nose radius tool reached higher stresses at the surface because of possessing higher initial surface residual stresses. Consequently, after the first loading cycle, higher plastic strains were generated. This implies that the specimens machined with the 1.2 mm nose radius tool were cycling with higher mean plastic strains than the specimens machined with the 4 mm nose radius tool, although the final surface residual stresses were lower.

4.3.Local fatigue approach

As previously discussed the stress-strain properties of the surface layer were modified due to the work hardening produced by the cutting process. Therefore, the maximum stress and minimum stress at the surface layer differed substantially from the maximum and minimum nominal stresses applied in the core region. Beyond this context, it seems possible to use a local fatigue approach in order to analyse the isothermal LCF fatigue behaviour of machined specimens. This local approach should take into account: local stress-strain properties of the surface layer, initial surface residual stresses and the topography of the surface region.

Both machined discs exhibited similar degree of work-hardening as revealed by the microstructure observations. Therefore, it can be assumed that the stress-strain properties of the surface layer are identical in both discs. Due to the difficulty of obtaining accurate stress-strain properties of the surface layer, these can be estimated based on the study published in [18]. In that study, under

similar cutting conditions to those employed in this work, the yield stress of the surface region was 1.8 times higher than the core region. In a recent study, Ding et al. [26] also reported that the yield stress of the machining-affected layer in the nickel based alloy RR1000 was near twice of the bulk. Figure 11 shows the stress-strain properties of the surface layer for both machined discs at 450. It should be noted that the stress is normalised with respect to the yield stress of the core region ($\sigma_{y,core}$).

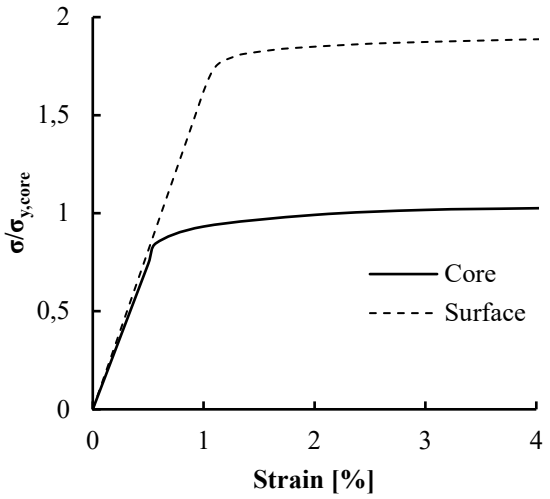

Figure 11. Estimated stress-strain properties of the surface layer and measured stress-strain properties of the core region at 450 ºC.

When applying a s^{ld} load the section of the specimen is subjected to a e_1 applied strain. Then, the $\varepsilon_{t,surf}$ total strain exhibited by the surface layer can be calculated employing eq.5, where E is the Young's modulus and $\sigma^{RS}_{surf,0}$ is the initial surface residual stress. Once the $\varepsilon_{t,surf}$ total strain exhibited by the surface layer is determined, the $\sigma_{surf,1}$ stress in the surface layer is obtained employing the stress-strain properties of the surface layer.

$$\varepsilon_{t,surf} = \varepsilon_1 + \frac{\sigma^{RS}_{surf,0}}{E} \qquad \text{(eq.5)}$$

The effect of the surface topography can be studied employing the fatigue stress concentration factor (k_f). For that purpose, the applied maximum strain energy $\sigma_{surf,1}\varepsilon_{t,surf}$ is multiplied by the fatigue

stress concentration k_f and equalled to the local strain energy $\sigma'_{surf,max}\,\varepsilon'_{t,surf}$ as expressed in eq.6. Doing so the maximum applied stress in the surface layer ($\sigma'_{surf,max}$) is obtained.

$$k_f \sigma_{surf,1} \varepsilon_{t,surf} = \sigma'_{surf,max}\,\varepsilon'_{t,surf} \qquad \text{(eq.6)}$$

Figure 12 shows the correlation between the maximum stress in the surface layer and the isothermal LCF fatigue life of both machined discs. The maximum stress in the surface layer was estimated using the methodology described in the preceding paragraphs. The correlation is quite good as the points of specimens from both discs follow almost the same correlation line. It can be concluded that the local approach can be useful to correlate surface integrity parameters (surface roughness, surface residual stresses and modified stress-strain properties of the surface) with fatigue behaviour. Nevertheless, it should be clarified that this model would not predict accurately the fatigue performance of specimens were cracks are initiated in carbide break outs as reported by [7,8] since the involved mechanisms are different.

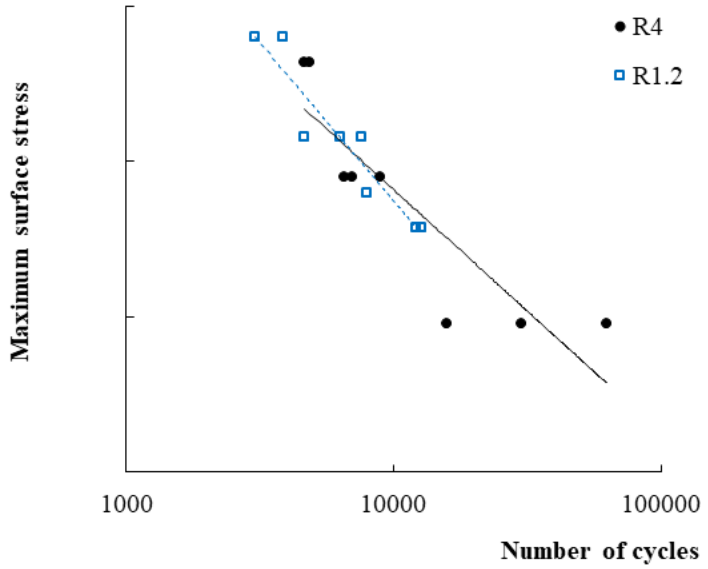

Figure 12. Correlation between the maximum surface stress in the surface layer and the isothermal LCF fatigue life of the machined discs.

6. Conclusions

In this work the surface integrity and low cycle fatigue life at 450 ºC of specimens obtained from two forged Inconel 718 discs which were face turned with 1.2 mm nose radius and 4 mm nose radius coated cemented carbide tools were analysed. The main conclusions gained from this study are:

- Specimens from both discs did not present significant microstructural alterations. The main defects were distorted layers and strain hardened layers, which did not exceed 10 μm depth, far from the acceptance limit defined by aero-engine manufacturers.
- Discs machined with 1.2 mm nose radius tools produced worst surfaces as they produced rougher surfaces and higher tensile residual stresses. When employing the 1.2 mm nose radius tool, Ra, R_z, R_t, and R_p roughness parameters were almost four times greater than 4 mm nose radius tools. Surface residual stresses were also %30-40 higher in the specimens manufactured with 1.2 mm nose radius tools.
- Specimens obtained from discs machined with the 4 mm nose radius exhibited longer LCF fatigue life at 450 ºC. Considering the shortest lives of each specimen batch at the same stress level, the specimens extracted from the disc machined with the largest nose radius tool led to 1.3-1.4 times longer lives. These results are in agreement with the better surface integrity generated with the 4 mm nose radius at the studied cutting conditions.
- The fracture analysis revealed that the surface state was the dominant factor and therefore a local approach was used to understand the influence of surface integrity (surface roughness, surface residual stresses and altered stress-strain properties of the surface layer) on the isothermal LCF fatigue behaviour of both machined discs. A satisfactory correlation was found between the maximum applied stress in the surface layer and the isothermal LCF fatigue life employing the local approach. It should be noted, that a different model should be used to predict fatigue behaviour of cracks initiated by carbide breakouts observed in other research works.

Data availability

Due to the interests of the industrial company involved in this project, the raw data would remain confidential and would not be shared.

Aknowledgment

The authors thank the Basque Government for the financial support given to the project FRONTIERS (KK-2019/00077).

References

[1] Posavljak, S., Maksimović, K. (2011). Initial fatigue life estimation in aero engine discs. Sci Tech Rev, 61(1), 25-30.

[2] Teti, R., et al. (2010). Advanced monitoring of machining operations. CIRPAnn-Manuf Technol, 59(2), 717-739. https://doi.org/10.1016/j.cirp.2010.05.010

[3] Ezugwu, E. O. (2004). High speed machining of aero-engine alloys. J Braz Soc Mech Sci Eng, 26(1), 1-11. https://doi.org/10.1590/S1678-58782004000100001

[4] Ulutan, D., Ozel, T. (2011). Machining induced surface integrity in titanium and nickel alloys: A review. Int J Mach Tools Manuf, 51(3), 250-280. https://doi.org/10.1016/j.ijmachtools.2010.11.003

[5] Thakur, A., and S. Gangopadhyay (2016). State-of-the-art in surface integrity in machining of nickel based super alloys. Int J Mach Tools Manuf,100:25-54. https://doi.org/10.1016/j.ijmachtools.2015.10.001

[6] Connolley, T., Starink, M. J., Reed, P. A. S. (2004). Effect of broaching on high-temperature fatigue behavior in notched specimens of INCONEL 718. Metall Mater Trans A, 35(3), 771-783. https://doi.org/10.1007/s11661-004-0005-z

[7] Bhowal, P. R., Stolz, D., Wusatowska-Sarnek, A. M., Montero, R. (2008). Surface effects on low cycle fatigue behavior in IN718 alloy. In 11th International Symposium on Superalloys, Superalloys. https://doi.org/10.7449/2008/Superalloys_2008_417_423

[8] Welling, D. (2014). Results of surface integrity and fatigue study of wire-EDM compared to broaching and grinding for demanding jet engine components made of Inconel 718. Procedia CIRP, 13, 339-344. https://doi.org/10.1016/j.procir.2014.04.057

[9] Herbert, C., Axinte, D.A., Hardy, M., Withers, P., (2014). Influence of surface anomalies following hole making operations on the fatigue performance for a nickel based superalloy. J Manuf Sci Eng, 136(5), 051016. https://doi.org/10.1115/1.4027619

[10] Andrews, R. G., Koul, A. K., Au, P. (1991). Fatigue crack initiation in alloy 718 at 650° C. Superalloys 718, 625 and Various Derivatives, 943-954. https://doi.org/ 10.7449/1991/Superalloys_1991_943_954

[11] Chen, Z., Moverare, J., Peng, R. L., Johansson, S. (2016). Surface integrity and fatigue performance of Inconel 718 in wire electrical discharge machining. Procedia CIRP, 45, 307-310. https://doi.org/10.1016/j.procir.2016.02.053

[12] Huang, Q., Ren, J. X. (1991). Surface integrity and its effects on the fatigue life of the nickel-based superalloy GH33A. Int J Fatigue, 13(4), 322-326. https://doi.org/10.1016/0142-1123(91)90359-7

[13] Bellows, G. (1972). Applying surface integrity principles in jet engine production. Met Eng Q, 12, 55-58.

[14] Ardi, D. T., Li, Y.G., Chan, K.H.K, Blunt, L., Bache, M.R., (2015). Surface topography and the impact on fatigue performance. Surf Topogr: Metrolog Prop, 3(1), 015007. https://doi.org/10.1088/2051-672X/3/1/015007

[15] Koster, W. P., Field, M., Fritz, L.J., Gatto, L.R., Kahles, J.F., (1970). Surface integrity of machined structural components (No. 970-11700), Metcut Research Associates Inc Cincinnati Oh

[16] Galatolo, R., Fanteria, D. (2017). Influence of turning parameters on the high-temperature fatigue performance of Inconel 718 superalloy. Fatigue Fract Eng Mater Struct, 40(12), 2019-2031. https://doi.org/10.1111/ffe.12623

[17] Hua, Y., Liu, Z. (2018). Experimental Investigation of Principal Residual Stress and Fatigue Performance for Turned Nickel based Superalloy Inconel 718. Mater, 11(6), 879. https://doi.org/10.3390/ma11060879

[18] Madariaga, A., Esnaola, J.A, Arrazola, P.J., Ruiz-Hervias, J., Muñoz, P., Ostolaza, K. (2015). Stability of machining induced residual stresses in Inconel 718 under quasi-static loading at room temperature. Mater Sci Eng A, 620, 129-139. https://doi.org/10.1016/j.msea.2014.09.118

[19] Prevéy, P (1986). The use of Pearson VII distribution functions in X-ray diffraction residual stress measurement. Adv X-Ray Anal, 29 (1986), 103-111. https://doi.org/10.1154/S037603080001017X

[20] Novovic, D., Dewes, R. C., Aspinwall, D. K., Voice, W., Bowen, P. (2004). The effect of machined topography and integrity on fatigue life. Int J Mach Tools Manuf, 44(2-3), 125-134. https://doi.org/10.1016/j.ijmachtools.2003.10.018

[21] Arola, D., Williams, C. L. (2002). Estimating the fatigue stress concentration factor of machined surfaces. Int J Fatigue, 24(9), 923-930. https://doi.org/10.1016/S0142-1123(02)00012-9

[22] Peterson, R. Stress concentration factors. John Willey & Sons, New (1974).

[23] J. Liu, H. Yuan (2010). Prediction of residual stress relaxations in shot-peened specimens and its application for the rotor disc assessment. Mater Sci Eng A 527(24), 6690-6698. https://doi.org/10.1016/j.msea.2010.07.010

[24] Manson, S., and Halford, G. Fatigue and durability of metals at high temperatures. ASM International, 2009.

[25] Madariaga, A., Aperribay, J., Arrazola, P. J., Esnaola, J. A., Hormaetxe, E., Garay, A., Ostolaza, K. (2017). Effect of Thermal Annealing on Machining-Induced Residual Stresses in Inconel 718. J Mater Eng Perform, 26(8), 3728-3738. https://doi.org/10.1007/s11665-017-2824-2

[26] Ding, R., Knaggs, C., Li, H., Li, Y. G., Bowen, P (2020). Characterization of plastic deformation induced by machining in a Ni-based superalloy. Mater Sci Eng A 778 (19), 139104. https://doi.org/10.1016/j.msea.2020.139104